Scintillation, Afterglow and Thermoluminescence of CsI:Tl,Sm

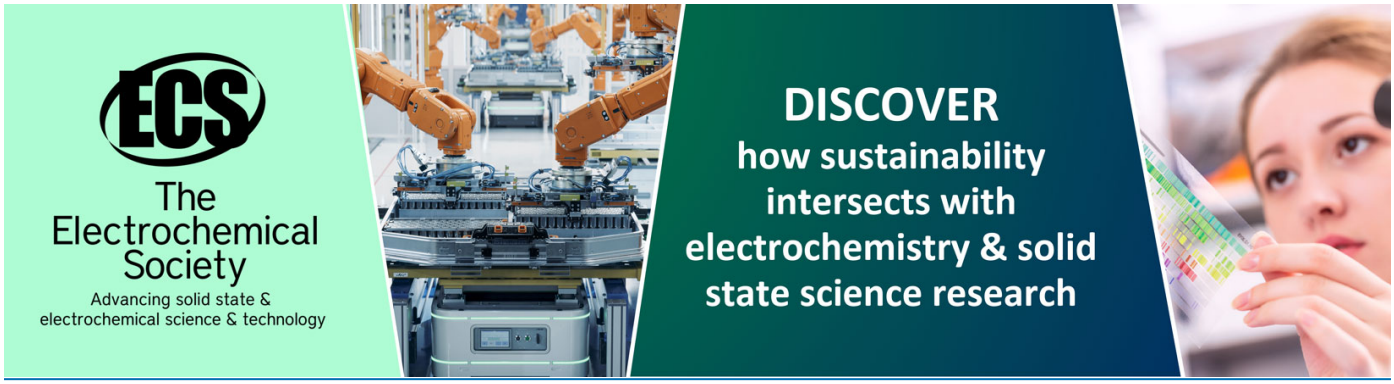

IOP Conf. Series: Materials Science and Engineering **15** (2010) 012091 doi:10.1088/1757-899X/15/1/012091

Scintillation, Afterglow and Thermoluminescence of CsI:Tl,Sm

L A Kappers[1], R H Bartram[1], D S Hamilton[1], A Lempicki[2], C Brecher[2], V Gaysinskiy[3], E E Ovechkina[3] and V V Nagarkar[3]

[1] Department of Physics, University of Connecticut, Storrs, CT 06269-3046, USA

[2] ALEM Associates, 44 Hunt St., Watertown, MA 02472, USA

[3] Radiation Monitoring Devices (RMD) Inc., 44 Hunt St., Watertown, MA 02472, USA

E-mail: lawrence.kappers@uconn.edu

Abstract. Experiments on co-doped CsI:Tl,Sm suggest that samarium electron traps scavenge electrons from thallium traps and that electrons subsequently released by samarium recombine non-radiatively with trapped holes, thus suppressing afterglow. These experiments support the inference that electrons tunnel freely between samarium ions and are trapped preferentially as substitutional Sm^+ near $V_{KA}(Tl^+)$ centers where non-radiative recombination is the rate-limiting step. Combined radioluminescence, afterglow and thermoluminescence on single-crystal samples of CsI:Tl and CsI:Tl,Sm, recorded sequentially at adjusted gain settings following low-temperature irradiation, reveal reversible radiation damage as well.

1. Introduction

The feasibility of substantially diminishing afterglow in CsI:Tl scintillator material by co-doping with Sm^{2+} has been demonstrated. [1] Rate equations informed by experiment predict that deeper samarium electron traps, involving diffuse 6*s* orbitals of Sm^+, scavenge electrons from shallower thallium traps, and combined radioluminescence, afterglow and thermoluminescence experiments on single-crystal samples of CsI:Tl,Sm suggest that most electrons released by Sm^+ recombine non-radiatively with holes trapped as $V_{KA}(Tl^+)$ centers (V_K centers trapped at Tl^+ ions), thus providing a mechanism for suppression of trapped-charge accumulation in repetitive applications. [2] A linear-coupling model in the harmonic approximation, based on quantum-chemistry calculations with selective lattice relaxation, suggests further that non-radiative charge transfer is enabled by low-energy excited states of Sm^{2+} within the ground configuration and is mediated by spin-orbit interaction. Although recombination is predominantly non-radiative, tracking of the process with enhanced gain settings is enabled both by radiative recombination following thermal ionization and by a small radiative component of the charge-transfer recombination associated with magnetic-dipole transitions from low-energy excited states of Sm^{2+}. In a previous investigation [3], combined scintillation and afterglow experiments were performed on single-crystal samples of CsI:Tl,Sm in order to determine the concentration dependence of the rate of non-radiative charge transfer and thus to construct a more nuanced model of the non-radiative process. The present investigation is concerned with the extension of these experiments to include thermoluminescence recorded at still another enhanced gain setting following both low-temperature irradiation and afterglow. Both CsI:Tl and CsI:Tl,Sm were investigated with and without optical filters.

2. Experiment

An electron Van de Graaff accelerator operated at a beam voltage of 1.0 MeV was employed as the primary radiation source with the 1.0 □A electron beam stopped by a thin copper target that served as a point source of 0.5 MeV gamma rays. Samples were mounted on a heated pedestal and cooled by flowing nitrogen gas, the sample temperature was monitored by a thermocouple and luminescence was conducted to a photomultiplier (PMT) by a shielded optical fiber. Following four-minute irradiations at -112 °C, the gain was increased by a factor of 10^3 to monitor the decay of the afterglow at constant temperature for ten minutes and then reduced by an additional factor of 10 to record thermoluminescence with a linear temperature ramp of 25 °C/min. Light-output data were recorded at four-second intervals both with and without a Schott orange OG530 optical filter in front of the PMT to suppress short wavelength radiation in an effort to discriminate between the activators for scintillation and for thermoluminescence, as explained in Section 5. Two single-crystal samples were investigated, one CsI:Tl and the other CsI:Tl,Sm. Nominal dopant concentrations were 0.11% Tl^+ in both samples and 0.05% Sm^{2+} in the second. Recorded light output is plotted in Figures 1 and 2.

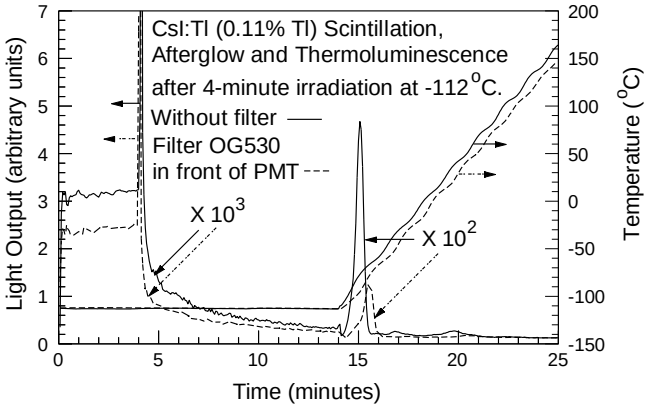

Figure 1. Scintillation, afterglow and thermoluminescence of CsI:Tl recorded at adjusted gain settings (left-hand scale) and sample temperature (right-hand scale) with (dashed curves) and without (solid curves) an OG530 optical filter inserted in front of the photomultiplier.

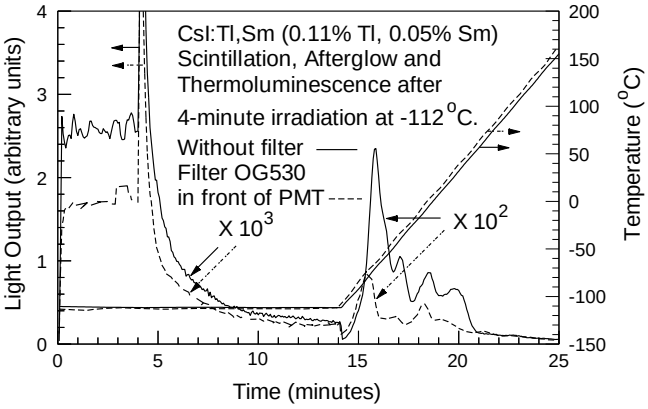

Figure 2. Scintillation, afterglow and thermoluminescence of CsI:Tl,Sm recorded at adjusted gain settings (left-hand scale) and sample temperature (right-hand scale) with (dashed curves) and without (solid curves) an OG530 optical filter inserted in front of the photomultiplier.

3. Rate Equations

Complete rate equations for the first two phases of the process were presented in Reference 2. Rate equations for the afterglow phase in terms of the normalized trapped-hole concentration $\tilde{n}_h$ and the normalized light output $\tilde{I}$ are

$$\frac{d\tilde{n}_h}{dt} \cong -p_e^{(Sm)}\tilde{n}_h - \alpha\tilde{n}_h^2, \tag{1}$$

$$\tilde{I} \cong -\frac{d\tilde{n}_h}{dt} - (1-r)\alpha\tilde{n}_h^2 = r\alpha\tilde{n}_h^2 + p_e^{(Sm)}\tilde{n}_h, \tag{2}$$

$$\alpha \cong s_A \exp(-E_A / k_B T), \tag{3}$$

$$p_e^{(Sm)} \cong s^{(Sm)} \exp(-E^{(Sm)} / k_B T), \tag{4}$$

with explicit solution as a function of afterglow time *t* for fixed temperature *T*:

$$\tilde{n}_h \cong \frac{\tilde{n}_{ho}\exp[-p_e^{(Sm)}t]}{1+[\alpha\tilde{n}_{h0}/p_e^{(Sm)}]\{1-\exp[-p_e^{(Sm)}t]\}}. \tag{5}$$

The parameters α and *r* respectively determine the rate of charge-transfer recombination and its radiative fraction, and the parameter $p_e^{(Sm)}$ determines the rate of thermal ionization. Both α and $p_e^{(Sm)}$ are of Arrhenius form. The parameter E_A can be identified with the thermal barrier for the non-radiative charge-transfer transition, while $s^{(Sm)}$ and $E^{(Sm)}$ are, respectively, the frequency factor and trap depth for thermal ionization. These equations were fitted to afterglow data in Reference 3 with the optimized parameters listed in Table 1. Optimized values of *r* are typically ~1%.

Table 1. Optimized parameters for thermally activated processes

%Sm^{2+}	E_A (eV)	s_A (min^{-1})	$E^{(Sm)}$ (eV)	$s^{(Sm)}$ (min^{-1})
0.2%	0.199	3.66×10^{5}	0.946	8.46×10^{13}
0.05%	0.180	5.26×10^{4}	0.925	8.48×10^{13}

4. Promoting-Interaction Model for Afterglow

The frequency factor s_A in Eq. (3) is proportional to the promoting interaction for the non-radiative charge-transfer transition (intersystem crossing) and thus to the square of the matrix element of the spin-orbit interaction between initial and final states. A diffuse 6s orbital centered at $\vec{r}_0$ can be represented in a continuum approximation with effective mass ratio $m^*/m \approx 1.0$ by

$$\phi_{6s}(\Delta r) = \frac{\exp(-\Delta r/\kappa a_0)}{\pi^{1/2}(\kappa a_0)^{3/2}},\ \Delta r \equiv |\vec{r} - \vec{r}_0|. \tag{6}$$

With the assumption of a fixed separation Δr of initial and final sites in each crystal sample, the ratio of promoting interactions is given by

$$\frac{s_{A1}}{s_{A2}} = \left[\frac{\phi_{6s}(\Delta r_1)}{\phi_{6s}(\Delta r_2)}\right]^2 = \exp[2(\Delta r_2 - \Delta r_1)/\kappa a_0], \quad (7)$$

$$\frac{\Delta r_2}{\Delta r_1} = \frac{\rho_1^{1/3}}{\rho_2^{1/3}} = 1.25, \quad (8)$$

where ρ is the total dopant concentration and $\kappa = 6.31$. It follows that $\Delta r_1 / a = 2.88$ and $\Delta r_2 / a = 3.59$, where $a = 4.56$ Å is the lattice parameter. These values are consistent with the inference that electrons tunnel freely between samarium ions and are trapped preferentially near $V_{KA}(Tl^+)$ centers (V_K centers trapped by Tl^+ ions) where non-radiative recombination is the rate-limiting step. An earlier tunnelling model of Delbecq *et al*. [4] provides an egregiously poor fit to the data; thus the data are not consistent with a random distribution of trapped electrons. [5]

5. Radiation-Damage Model for Thermoluminescence

Thermoluminescence with and without an optical filter reveals glow peaks at an appreciably shorter wavelength than that of the Tl^+ emission during scintillation and afterglow, as is evident from Table 2. The smaller reduction in Scint ratio with addition of Sm^{2+} is attributed to a slight shift of scintillation light output to shorter wavelengths [1]. A single glow peak is observed in CsI:Tl in Figure 1 and multiple glow peaks in CsI:Tl,Sm in Figure 2. Excitons efficiently transport energy to Tl^+ activators during room-temperature irradiation, but they become self-trapped and decompose into *F-H* pairs during low-temperature irradiation. The more mobile *H* centers are subsequently trapped at Tl^+ as $H_A(Tl^+)$ centers or at Sm^{2+} as $H_A(Sm^{2+})$ centers perturbed by charge-compensating cation vacancies V_C^- in various relative locations, until they are thermally released and recombine with *F* centers. *Ab initio* calculations suggest that the deepest traps correlate with the most remote cation vacancies. The observed glow peaks are tentatively attributed to radiative recombination events. [6], [7]

Table 2. Ratios of integrated light output with and without the OG530 filter.

Sample	Scint ratio	TL ratio
CsI:Tl	0.77	0.44
CsI:Tl,Sm	0.67	0.44

Thermoluminescence glow peaks were least-squares fit to appropriate theoretical expressions [8] as shown in Figures 3a and 3b, with optimized parameter values listed in Table 3.

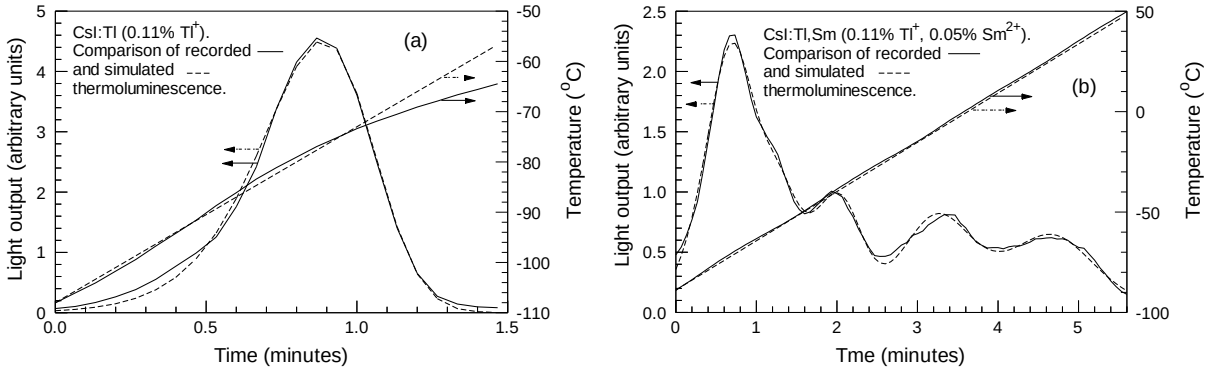

Figure 3. Recorded and simulated thermoluminescence for (a) CsI:Tl and (b) CsI:Tl,Sm.

The simulated thermoluminescence in Figure 3 is derived from the interpolation formula [8]:

$$\tilde{I} = -\frac{d\tilde{n}}{dt} = \tilde{n}^b p, \quad 1 \le b \le 2, \tag{9}$$

$$p = s\exp(-E/k_B T), \tag{10}$$

where $\tilde{I}$ is the light output and $\tilde{n}$ is the concentration of trapped charges, both normalized to the trap concentration *N*, *s* is the frequency factor, *E* is the trap depth and *b* is the order of kinetics.

Table 3. Optimized parameters for Figures 3a and 3b. The size parameter *B* is the fractional contribution of each component glow curve to the total thermoluminescence.

Sample	Trap	Kinetic order *b*	*E*(eV)	$s(10^{14}$ min$^{-1})$	Size *B*
CsI:Tl	Tl^+	1.15	0.532	3.68	1.0
CsI:Tl,Sm	Tl^+	1.2	0.543	2.36	0.268
CsI:Tl,Sm	$Sm^{2+}(1)$	1.3	0.602	11.5	0.175
CsI:Tl,Sm	$Sm^{2+}(2)$	1.4	0.677	33.0	0.169
CsI:Tl,Sm	$Sm^{2+}(3)$	1.8	0.734	10.8	0.194
CsI:Tl,Sm	$Sm^{2+}(4)$	1.9	0.805	4.15	0.184

The properties of the first trap in CsI:Tl,Sm are essentially identical with those of the single trap in CsI:Tl; accordingly, it is assigned to the Tl^+ center. The four remaining traps are then assigned to perturbed Sm^{2+} centers by default. Note that the kinetic order *b* increases monotonically with trap depth, corresponding to an enhanced probability of re-trapping in deeper traps.

6. Discussion

The calculated values for the separation of initial and final sites are plausible for the nearest dopant sites but not for a random distribution of trapped charges substantially less than the dopant concentration, thus explaining the single non-radiative transition rate during the afterglow phase for fixed temperature and dopant concentration. Glow peaks observed during the thermoluminescence phase following low-temperature irradiation provide evidence of reversible radiation damage.

As noted previously, scintillator samples were cooled by flowing nitrogen gas. It was not feasible with the existing apparatus to cool them rapidly or to cool them to liquid nitrogen temperature. However, the present experiment was motivated in part by the observation of anomalously persistent afterglow in CsI:Tl,Sm at certain temperatures which was tentatively attributed to radiation damage. The observation of thermoluminescence beginning at the same temperature as the persistent afterglow served to confirm that conjecture, and thus proved advantageous.

Acknowledgements

We thank NIH and DOE for support of this work under Grants No. 5R44RR022921-03, 1R44RR025286-01 and DE-FG02-06ER84434.

References

[1] Nagarkar V V, Brecher C, Ovechkina E E, Gaysinskiy V, Miller S R, Thacker S, Lempicki A and Bartram R H 2008 Scintillation properties of CsI:Tl crystals codoped with Sm^{2+} *IEEE Transactions on Nuclear Science* **55** 1270-1274

[2] Bartram R H, Kappers L A, Hamilton D S, Lempicki A, Brecher C, Gaysinskiy V, Ovechkina E E and Nagarkar V V 2008 Afterglow suppression and non-radiative charge-transfer in CsI:Tl,Sm *IEEE Transactions on Nuclear Science* **55** 1232-1236

[3] Kappers L A, Bartram R H, Hamilton D S, Lempicki A, Brecher C, Gaysinskiy V, Ovechkina E

E and Nagarkar V V Concentration dependence of afterglow suppression in CsI:Tl,Sm *Journal of Physics: Conference Series* (in press)

[4] Delbecq C J, Toyozawa Y and Yuster P H 1974 Tunneling recombination of trapped electrons and holes in KCl:AgCl and KCl:TlCl *Phys. Rev. B* **9** 4497

[5] Kappers L A, Bartram R H, Hamilton D S, Lempicki A, Brecher C, Gaysinskiy V, Ovechkina E E, Thacker S and Nagarkar V V 2010 A tunneling model for afterglow suppression in CsI:Tl,Sm scintillation materials *Radiation Measurements* **45** 426-428

[6] Falco J, Von der Weid J P, Aegerter M A, Iida T and Nakaoka T 1980 Self-trapped excitons in caesium-iodide. II. Magneto-optical properties. *Journal of Physics C* **13** 993

[7] Song K S and Williams R T 1993 *Self-Trapped Excitons* (Berlin, Heidelberg: Springer)

[8] Chen R and McKeever S W S 1997 *Theory of Thermoluminescence and Related Phenomena* (Singapore: World Scientific)